Relative contributions of temperature and salinity to seasonal mixed layer density changes and horizontal density gradients

Gregory C. Johnson,[1] Sunke Schmidtko,[1,2] and John M. Lyman[1,3]

Received 30 September 2011; revised 17 February 2012; accepted 21 February 2012; published 10 April 2012.

[1] Temperature and salinity both contribute to ocean density, including its seasonal cycle and spatial patterns in the mixed layer. Temperature and salinity profiles from the Argo Program allow construction and analysis of a global, monthly, mixed layer climatology. Temperature changes dominate the seasonal cycle of mixed layer density in most regions, but salinity changes are dominant in the tropical warm pools, Arctic, and Antarctic. Under the Intertropical Convergence Zone, temperature and salinity work in concert to increase seasonal stratification, but the seasonal density changes there are weak because the temperature and salinity changes are small. In the eastern subtropics, seasonal salinity changes partly compensate those in temperature and reduce seasonal mixed layer density changes. Besides a hemispheric seasonal reversal, the times of maximum and minimum mixed layer density exhibit regional variations. For instance, the equatorial region is more closely aligned with Southern Hemisphere timing, and much of the North Indian Ocean has a minimum density in May and June. Outside of the tropics, the maximum mixed layer density occurs later in the winter toward the poles, and the minimum earlier in the summer. Finally, at the times of maximum mixed layer density, some of the ocean has horizontal temperature and salinity gradients that work against each other to reduce the horizontal density gradient. However, on the equatorial sides of the subtropical salinity maxima, temperature and salinity gradients reinforce each other, increasing the density gradients there. Density gradients are generally stronger where either salinity or temperature gradients are dominant influences.

Citation: Johnson, G. C., S. Schmidtko, and J. M. Lyman (2012), Relative contributions of temperature and salinity to seasonal mixed layer density changes and horizontal density gradients, *J. Geophys. Res.*, *117*, C04015, doi:10.1029/2011JC007651.

1. Introduction

[2] The evolution of the seasonal mixed layer is influenced by a variety of phenomena, including air-sea heat flux [e.g., *Yu and Weller*, 2007], air-sea freshwater flux (or evaporation minus precipitation) [e.g., *Schanze et al.*, 2010; *Yu*, 2011], air-sea momentum fluxes [e.g., *Risien and Chelton*, 2008], continental [e.g., *Dai and Trenberth*, 2002] and sea-ice [e.g., *Häkkinen*, 1993] contributions to the freshwater flux, turbulent and convective mixing of water properties from below [e.g., *Price et al.*, 1986], the structure of the water properties below including barrier layers [e.g., *de Boyer Montégut et al.*, 2007], horizontal and vertical advection of water properties [e.g., *Hosegood et al.*, 2008], and even variations in light penetration [e.g., *Ohlmann et al.*, 1996]. Given strong regional variations in all of these phenomena and their seasonal cycles, the properties of the seasonal mixed layer and their seasonal evolution vary widely.

[3] Seasonal mixed layer stratification and erosion influence biological production by governing the depth and amount of nutrients available within the euphotic zone [e.g., *Fasham et al.*, 1990], along with other factors. Seasonal mixed layer stratification here means the changes in surface mixed layer density (owing to changes in temperature and salinity) between the time of maximum density (usually late winter or early spring) and that of minimum mixed density (usually late summer or early fall). These processes also have strong influences on air-sea gas exchange, including oxygen and carbon dioxide [e.g., *Peng et al.*, 1987], which are biologically and biogeochemically important dissolved gasses. Hence, understanding and quantifying regional variations of seasonal stratification and erosion including their strength, timing, and the relative contributions of temperature and salinity are of wide interest.

[4] Mixed layer properties at the times of maximum density (late winter in most locations) have a strong influence on subsurface ocean properties because it is when the mixed layer is deepest and densest that it communicates most effectively with the ocean interior, primarily by subduction of mixed layer water into the ocean interior [*Stommel*, 1979]. In this manner, late winter mixed layer properties help to set

[1]Pacific Marine Environmental Laboratory, NOAA, Seattle, Washington, USA.
[2]Now at School of Environmental Sciences, University of East Anglia, Norwich Research Park, Norwich, UK.
[3]Joint Institute for Marine and Atmospheric Research, University of Hawai'i at Manoa, Honolulu, Hawaii, USA.

0148-0227/12/2011JC007651

the interior ocean structure of temperature, salinity, and density.

[5] Previous studies have focused on quantifying mixed layer depth [e.g., *Kara et al.*, 2003; *de Boyer Montégut et al.*, 2004]. Here we use Conductivity-Temperature-Depth (CTD) instrument data from the Argo array and other sources to investigate several aspects of the relative roles of temperature and salinity in the seasonal cycle of the mixed layer. We analyze these properties at times of maximum mixed layer density because of their importance in setting interior ocean structure where water is subducted. In some other locations, barrier layers can insulate the ocean interior from the mixed layer. Barrier layers are prominent and semipermanent in much of the fresher regions of the tropics [e.g., *Lukas and Lindstrom*, 1991; *Sprintall and Tomczak*, 1992; *Mignot et al.*, 2007] and in more localized fresher high-latitude regions [e.g., *de Boyer Montégut et al.*, 2007]. We discuss the differences of the properties between the times of minimum and maximum mixed layer density because these changes allow assessment of their relative roles in setting the seasonal stratification. We also examine the seasonal timing of these extrema in mixed layer density, pointing out that it varies subtly with latitude and also departs more radically from the canonical late spring and late winter times in a few regions. Finally, we examine the relative roles of temperature and salinity in setting horizontal density gradients during the times of maximum mixed layer density to quantify where and how much these gradients reinforce or compensate each other in contributing to the lateral density gradient, which in turn contributes to the strength and location of surface fronts.

2. Data and Methods

[6] Argo [*Roemmich et al.*, 2009] is a global ocean array of autonomous profiling CTD floats with a target spacing of 3° latitude by 3° longitude. Each float reports profiles of temperature, salinity, and pressure between the surface and a target pressure of 2000 dbar at nominal 10 day intervals. The initial target number of active floats for the deep (>2000 m) ice-free ocean excluding marginal seas was 3000. Argo began in 1999, and reached 3000 active floats by November 2007, including some floats in marginal seas, and some in the seasonally ice-covered ocean.

[7] Year-round global sampling of upper ocean temperature and salinity by Argo has revolutionized oceanography, enabling studies such as this one into the seasonal evolution of the mixed layer during about 2000–2010. However, for true global coverage the Argo array must expand onto the continental shelves, into marginal seas, into the seasonally and year-round ice-covered regions of the oceans, and to the ocean floor. To address these deficiencies, archived shipboard CTD data from WOD 2009 [*Boyer et al.*, 2009] and CTD data from Ice-Tethered Profilers (ITPs) in the Arctic Ocean [*Toole et al.*, 2011] are here added to the Argo data set. While the Argo and ITP CTD data are centered on the past decade, we incorporate historical shipboard CTD data from as early as 1970 to increase coverage in these areas still under- or unsampled by Argo. Data are limited to quality-controlled relatively high-resolution CTD profiles from Argo floats, shipboard surveys, and ITPs to ensure simultaneous measurements of temperature and salinity with vertical resolution adequate to estimate the maximum mixed layer pressure.

[8] Mixed layer temperature, T, salinity, S, and maximum pressure, P (customarily referred to as the mixed layer depth), are estimated for each profile following *Holte and Talley* [2009]. Their multistep algorithm selects the bottom of the mixed layer based on the temperature and density profiles much as a well-trained analyst might. It is accurate in determining the mixed layer even in the presence of barrier layers and density-compensating near-surface layers. A climatological seasonal cycle at monthly resolution is constructed from the local estimates on a regular $0.5^\circ \times 0.5^\circ$ grid following S. Schmidtko et al. (Monthly Isopycnal/Mixed-layer Ocean Climatology (MIMOC), submitted to *Journal of Atmospheric and Oceanic Technology*, 2012). Their mapping incorporates detection of mixed layer density fronts, considers ocean bathymetry, thus effectively separating coastal from interior regions, and accounts for the equatorial waveguide. The mapping retains very fine lateral scale features, so a 5×5 point binomial-distribution spatial smoother is applied to the monthly T, S, and P fields prior to the analysis.

[9] The weighted number of observations for map grid points varies geographically (not shown). The zonally averaged values are lowest in the high latitudes in winter, falling below 10 south of around 64°S and north of around 76°N. In much of the Southern Hemisphere (from 58°S to 12°S) these values range between 40 and 50 on average. The zonally averaged values drop to around 30 around the equator. In the Northern Hemisphere these values are above 40 from 12°N to 60°N in all months, peaking around 80 near 48°N. Values in coastal regions are generally lower than the ocean interior except around the United States of America, much of Canada, Japan, and Europe, where there are many historical shipboard CTD data.

[10] The time of year at which the maximum mixed layer density occurs is found at each location from a cubic spline fit to the monthly maps, and the properties (T, S, and P) of that mixed layer for that time are found. The same procedure is used to find the times of year at which the minimum mixed layer density and the maximum mixed layer depth occur.

[11] The relative roles of changes in mixed layer T and S in determining how the surface mixed layer density, ρ, changes between the time of maximum and minimum density at any given location are quantified using a seasonal Turner angle, Tu_s:

$$Tu_s = \mathrm{atan2}(\alpha\Delta T + \beta\Delta S, \alpha\Delta T - \beta\Delta S),$$

where atan2 is the four-quadrant inverse tangent, α is the thermal expansion coefficient, β is the haline contraction coefficient, and Δ signifies the quantity at the time of maximum density minus its value at the time of minimum density. The quantities α and β are evaluated at surface pressure using the means of T and S at their times of minimum and maximum density for each location. This definition follows *Ruddick* [1983], where $Tu_s = 45^\circ$ indicates that temperature is the only contributor, -45° indicates that salinity is the only contributor, and the angles between indicate that both T and S are contributing together to the change, equally at 0°. In contrast, $Tu_s > 45^\circ$ indicates that S is working against T,

effecting complete compensation by 90°, and $Tu_s < -45°$ indicates that T is working against S, effecting complete compensation by $-90°$. A value of $|Tu_s| > 90°$ indicates an unstable condition, which is not applicable in this study. While Tu_s is evaluated using changes in time, it can be thought of as approximately reflecting the seasonal vertical stratification, with the properties at times of maximum density located below those at times of minimum density.

[12] Similarly, a horizontal Turner angle within the mixed layer, Tu_h, is defined as:

$$Tu_h = \text{atan2}\left(\frac{\nabla\rho}{|\nabla\rho|} \bullet (\alpha\nabla T + \beta\nabla S), \frac{\nabla\rho}{|\nabla\rho|} \bullet (\alpha\nabla T - \beta\nabla S)\right),$$

where ∇ signifies the horizontal gradient, $||$ the amplitude, and $\bullet$ the dot product. Taking the dot product to determine the components of the scaled sums and differences of salinity and temperature gradients (which are vectors) along the direction of the unit density gradient is an improvement on analyzing the meridional component of the Turner angle [e.g., *Chen*, 1995; *Tippins and Tomczak*, 2003], as surface density gradients are not constrained to be oriented purely north-south and the dynamically relevant component of the Turner angle lies along the density gradient (whether in vertical space, horizontal space, or even time—here seasonal).

3. Results

[13] This discussion starts with spatial patterns of the temperature, salinity, and density of the mixed layer at the times of maximum mixed layer density (usually late winter or early spring), and their relation to large-scale influences. It then focuses on patterns of changes in these mixed layer properties between these times and those of minimum mixed layer density (usually late summer or early autumn). This quantity is referred to as the seasonal stratification, and the relative roles of T and S in setting it are analyzed. Following that, the latitudinal variations of the seasonal timing of the minimum and maximum mixed layer densities (and maximum mixed layer depth), along with regions where this timing is unusual, are discussed. Finally, the spatial pattern of the magnitude of the horizontal density gradient at times of maximum mixed layer density and the relative roles of T and S in forming that gradient are addressed.

3.1. Mixed Layer Properties at the Annual Density Maximum

[14] Temperature at the times of maximum mixed layer density exceeds 28°C in the western tropical Pacific and eastern tropical Indian oceans, and generally trends cooler with increasing latitude, falling below 0°C in both the Arctic and Antarctic regions of the ocean (Figure 1a). Cold tongues near the equator in the eastern Pacific Ocean, and to a lesser extent the eastern Atlantic, are evident, resulting from a complex dynamical interplay [e.g., *Kessler et al.*, 1998]. The cold signature of coastal upwelling is evident in both hemispheres along the west coast of Africa [e.g., *Hagen et al.*, 2001] and along South America [e.g., *Sobarzo et al.*, 2007], but is less obvious along the west coast of North America [*Marchesiello et al.*, 2003]. The temperature at the time of minimum mixed layer density (nominally late summer, and not shown) generally exhibits a stronger coastal upwelling signature, consistent with seasonal cycles in the winds [e.g., *Bakun and Nelson*, 1991]. The strong contrast between the subtropical and subpolar gyres is especially evident at the western boundaries of the North Atlantic and North Pacific oceans, but also in the South Atlantic where the Brazil and Malvinas/Falkland Currents meet [e.g., *Gordon*, 1989], and even south of Africa where the Agulhas Current retroflects [*Lutjeharms and Van Ballegooyen*, 1988]. Even at the time of year when surface density is at a maximum (generally late winter), the relatively warm surface waters entering the Arctic Ocean [e.g., *Hansen and Osterhus*, 2000] are evident along the west coast of Northern Europe.

[15] Salinity (Figure 1b) maxima in all subtropical gyres reflect the dominance of evaporation over precipitation in those regions [*Schanze et al.*, 2010]. The relatively fresh belt north of the equator across the Pacific and Atlantic oceans (around 3°N–8°N) results in part from the strong precipitation in the Intertropical Convergence Zone (ITCZ), much as the fresh region in the western tropical South Pacific is related to the South Pacific Convergence Zone (SPCZ) [e.g., *Delcroix et al.*, 1996]. Salinity generally decreases in the higher latitudes as well, also reflecting the dominance of precipitation over evaporation in these locations. The high-latitude North Pacific is fresher than the North Atlantic because evaporation dominates over precipitation in the Atlantic, whereas the terms come closer to balancing in the Pacific. There is a strong contrast between the salty Arabian Sea, where the monsoon winds carry moisture from the oceans to the Indian subcontinent, and the relatively fresh Bay of Bengal, where precipitation and riverine freshwater sources have a strong effect on the mixed layer salinity [e.g., *Han and McCreary*, 2001]. The Mediterranean and Red seas are remarkably salty owing to the strong dominance of evaporation over precipitation there, as can even be inferred from the two-layer reverse estuarine exchanges between these arid marginal seas and the open ocean [e.g., *Bryden et al.*, 1994; *Johns et al.*, 2003]. Conversely, the surface mixed layer just west of Columbia and in the Gulf of Panama is remarkably fresh owing to strong precipitation in the region. As for temperature, the flow of salty water from the North Atlantic into the Arctic is evident along the west coast of Northern Europe, as is the fresh influence of the flow of Pacific waters into the Arctic through the Bering Strait [e.g., *Coachman and Aagaard*, 1988]. These salinity patterns generally hold throughout the year.

[16] The maximum mixed layer density reflects the influences of both temperature and salinity (Figure 1c). Its lowest values are found in the tropics where salinity is lowest, especially just west of Columbia in the Pacific and in the Bay of Bengal in the Indian Ocean, but also just north of the equator (under the ITCZ) across the Pacific and Atlantic. Density increases toward the poles, reaching high values in the Weddell and Ross seas of the Antarctic where the temperatures are very cold, and in the Arctic Ocean where salty Atlantic water influence is strong, also with cold temperatures. The saltier North Atlantic is much denser than the North Pacific [*Warren*, 1983]. Some of the highest densities are observed in the salty evaporation basins of the Mediterranean and Red seas, despite their relative warmth. Again, a slight influence of upwelling can be seen in the relatively dense coastal waters (compared to the interior waters at the same latitudes) off the west coasts of Africa and South

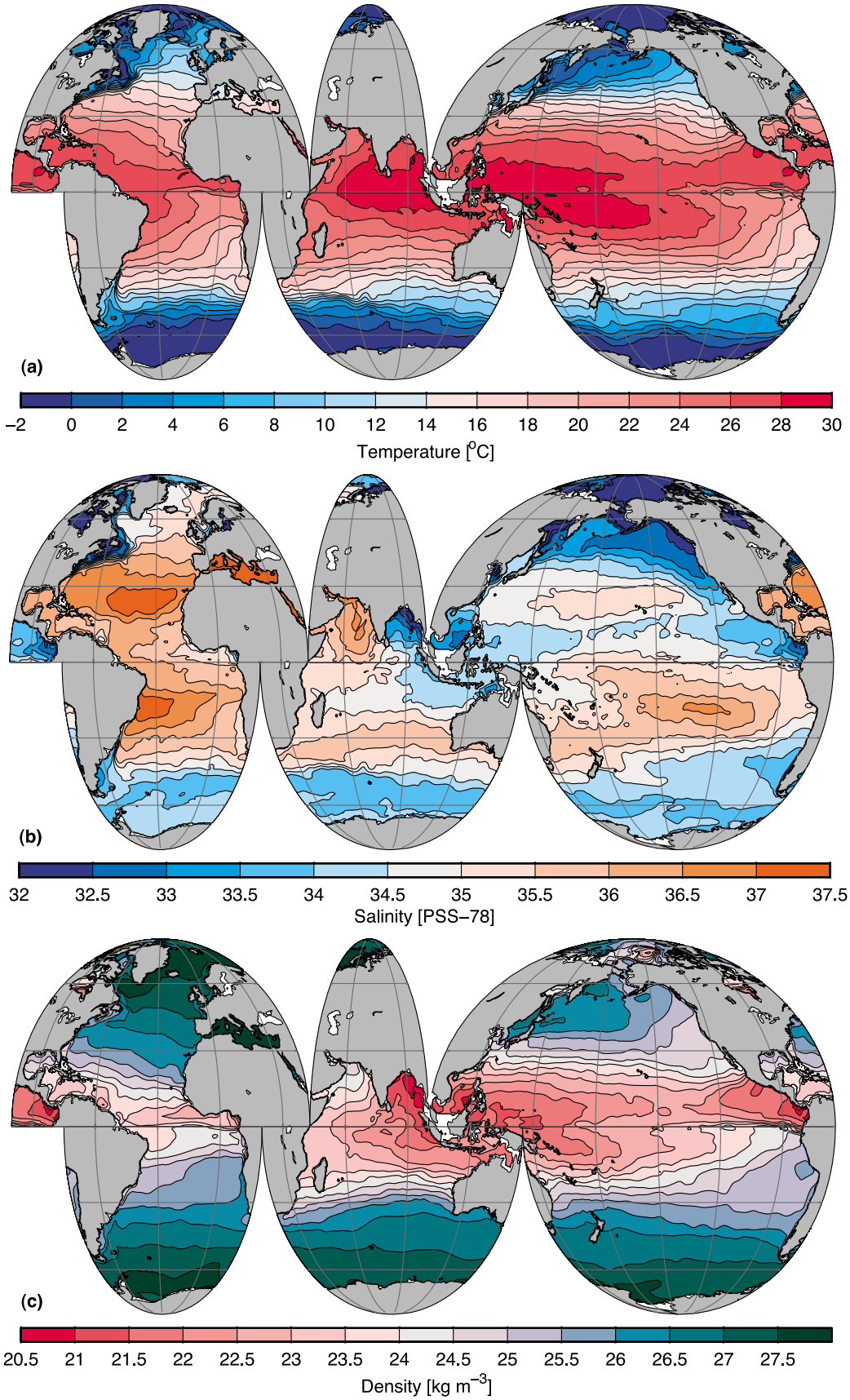

Figure 1. Maps of surface mixed layer (a) temperature, (b) salinity, and (c) density at times of its maximum density.

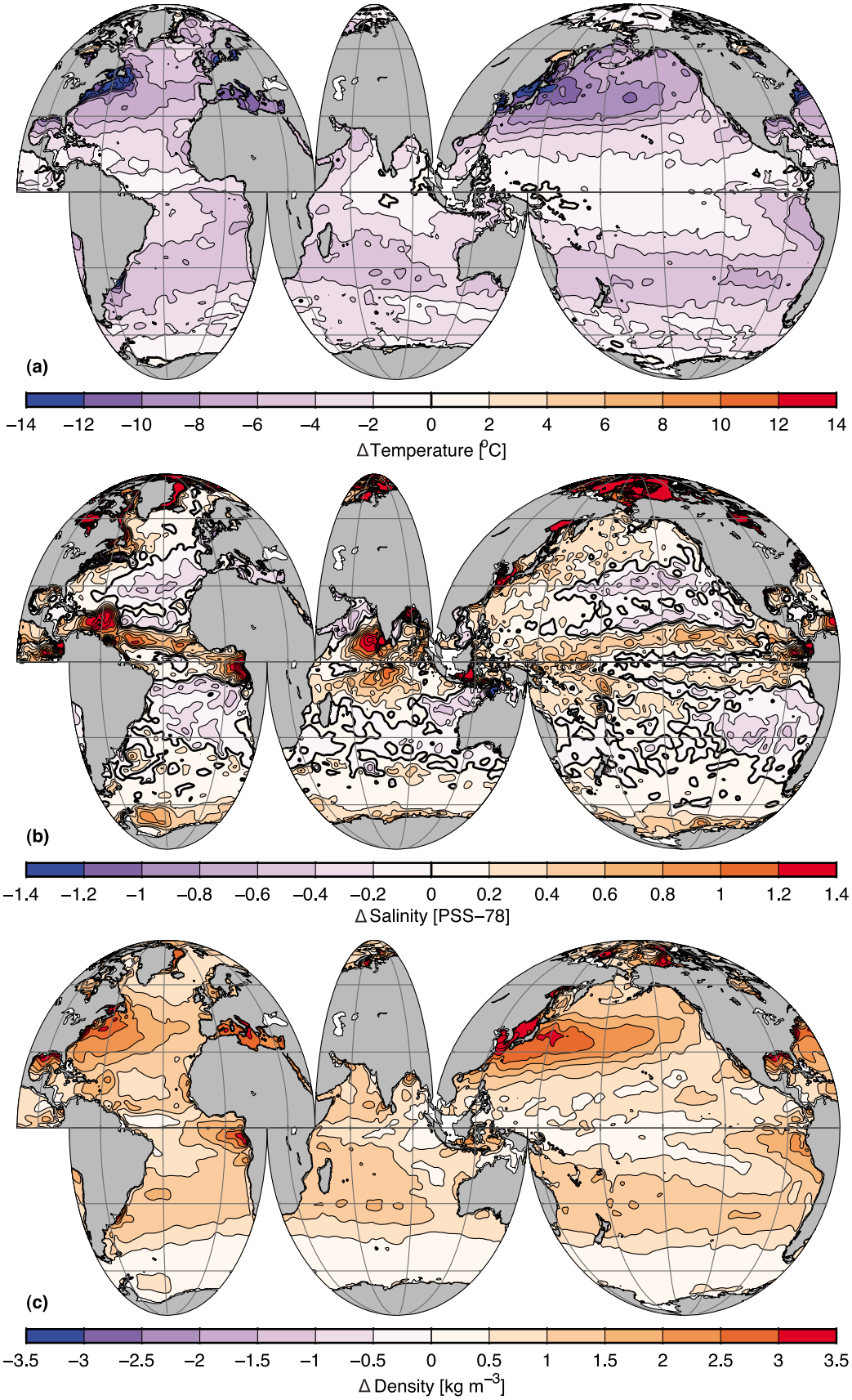

Figure 2. Maps of surface mixed layer properties at times of its maximum density minus those at its minimum density: (a) temperature, (b) salinity, and (c) density, all with thick black zero contours.

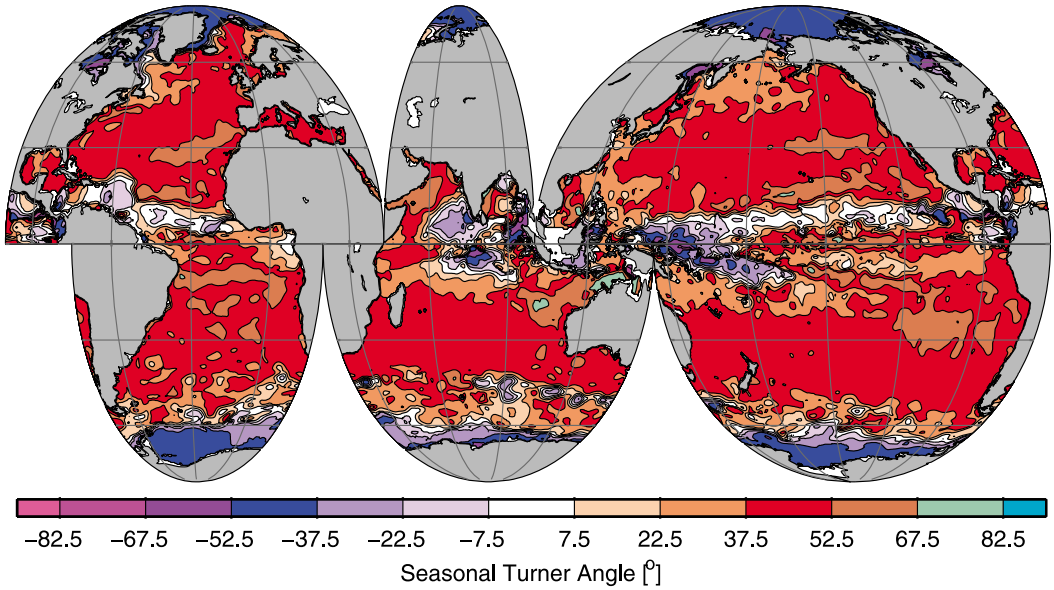

Figure 3. Map of seasonal Turner angle for times of maximum minus minimum surface mixed layer density.

America. This influence is stronger and more obvious, including in the North Pacific, at the times of the density minimum (not shown).

3.2. Mixed Layer Property Differences Between the Times of Mixed Layer Density Extrema

[17] The temperatures at the times of the seasonal maximum in mixed layer density minus those at the times of minimum density (Figure 2a) are small in magnitude across much of the tropics and subpolar regions, with larger changes in the subtropics. The lack of tropical temperature change reflects the relatively constant solar forcing in those regions, with the strongest changes being associated with the seasonal evolution of the cold tongue in the eastern Pacific and Atlantic oceans. The mixed layer is even warmer at times of maximum density than at times of minimum density in a few small isolated regions in the tropical fresh pools and at high latitudes, allowed by a salinity-dominated seasonal density cycle and phase differences between seasonal temperature and salinity extrema. The larger subtropical changes are biggest in the western boundary regions of the Northern Hemisphere oceans, with the South Atlantic east-west contrast in the subtropics being much less prominent, and with no visible South Indian or South Pacific subtropical east-west contrast. These east-west contrasts are owing to the strong ocean heat loss to cold continental air in winter [e.g., *Yu and Weller*, 2007], as is the strong change seen in the Mediterranean Sea. Off the low-latitude (but off-equatorial) west coasts of South America and Africa there is some temperature contrast due to upwelling, but at higher latitudes along these coasts (and the west coast of North America), there is less of a seasonal contrast because cold summer upwelling reduces the contrast of mixed layer temperatures there with winter conditions.

[18] Salinities at the time of the maximum density minus those at the times of minimum density (Figure 2b) are of both signs, with positive changes acting to increase the seasonal density difference, and negative changes acting to decrease the seasonal density difference (assuming temperature changes (Figure 2a) increase the seasonal density difference, as they do in all but a few small regions). Positive salinity changes are evident across the ITCZ and in the SPCZ, where seasonal precipitation changes are large. The northern Bay of Bengal, the central Indian Ocean south of the equator, the Arabian Sea west of Sri Lanka, the Gulf of Panama, and the Gulf of Guinea all exhibit large positive changes caused by a variety of terms including lateral advection, vertical entrainment, and air-sea fluxes [*Yu*, 2011]. Around Antarctica, salinity increases in winter, perhaps owing to brine rejection from sea ice, and vice versa in summer, owing to melting of sea ice [e.g., *Martinson*, 1990] and glacial ice. A similar and stronger phenomenon is obvious in the Arctic Ocean, where, in addition to seasonal sea ice freshwater storage influences, summer river run-off from Alaska, Canada, and Russia may increase the contrast [e.g., *Serreze et al.*, 2006]. Throughout much of the subtropics, salinity decreases during the winter tend to reduce the seasonal contrast in mixed layer density changes relative to what would result from temperature decreases alone. Although evaporation associated with strong trade winds removes fresh water during the buoyancy loss season in these regions, entrainment of fresher water within the seasonal pycnocline is important in reducing the salinity in the mixed layer [e.g., *Jenkins*, 1982; *Johnson*, 2006; *Yu*, 2011]. Similar effects are evident in the western Arabian Sea, owing to the strong wind-driven mixed layer entrainment during the Southwest Monsoon [e.g., *Prasad*, 2004], and in the Mediterranean Sea.

[19] The amplitude of the annual cycle in density (the difference of density at its times of maximum minus its times of minimum, Figure 2c) is largest in the western subtropics of the North Atlantic and North Pacific, where strong seasonal heat loss is important, and generally small in the tropics and higher latitudes. Density changes are also large in the eastern equatorial Pacific and Atlantic oceans, with temperature changes being important in both of these

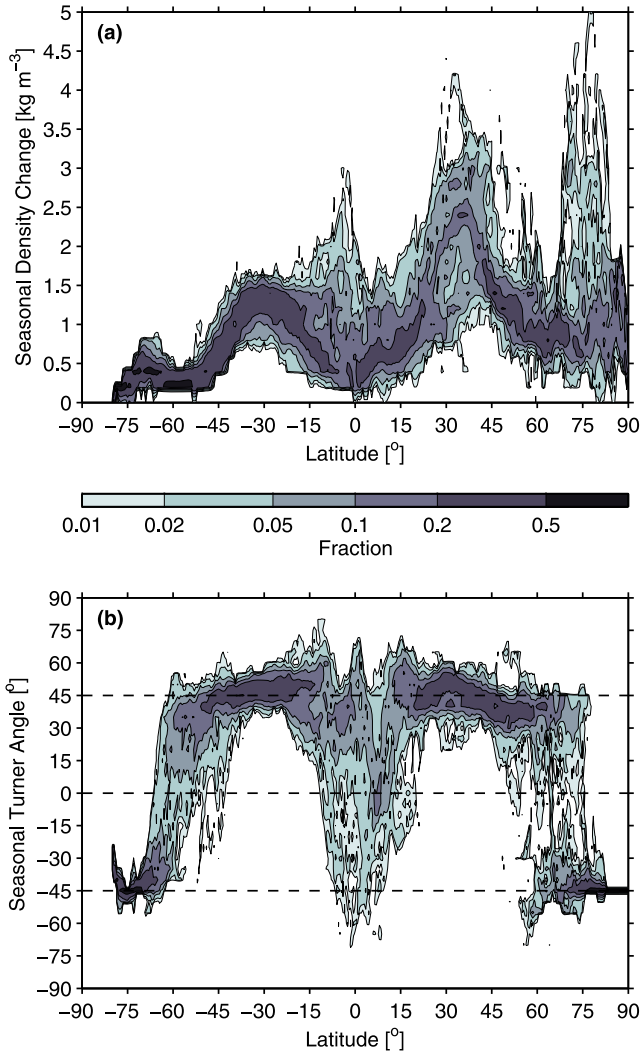

Figure 4. Fraction of surface mixed layer (a) seasonal density change in 0.2 kg m^{-3} bins and (b) seasonal Turner angle in 5° bins as a function of latitude, contoured at roughly logarithmic intervals.

regions, but salinity also important in the eastern equatorial Atlantic. Seasonal density changes are quite small off the subtropical west coasts of the Americas and Africa, likely owing to the influence of cold summertime upwelling regimes in these locations. East of Greenland and north of some regions of Russia, Canada, and Alaska, there are large seasonal density changes, mostly owing to large surface salinity changes as discussed above. Again, the evaporation basins of the Mediterranean and Red seas also show large seasonal density changes, especially the former.

[20] Calculating the seasonal Turner angle, Tu_s, to quantify the relative influences of salinity and temperature on seasonal density changes reveals that wide areas of the subtropics have $37.5° < Tu_s < 52.5°$, being regions where temperature changes predominantly influence the seasonal mixed layer density change (Figure 3). However, in the eastern subtropics, where eastern subtropical mode waters are formed, salinity plays a slightly destabilizing role in the seasonal surface density cycle with $Tu_s > 52.5°$, as it does in the western Arabian Sea. Again, these locations have a buoyancy loss season with strong, dry winds, inducing mixed layer cooling and salinification by evaporation, but entrainment of fresher water from the seasonal pycnocline into the mixed layer dominates the salinity change, with the resulting freshening working against cooling during the time period over which the mixed layer becomes denser.

[21] The tropics, with their weak seasonal cycle of density (Figure 2c), contain a wide range of relative roles for salinity and temperature in setting the density cycle (Figure 3). Salinity dominates in setting seasonal stratification in the tropical warm pools of the western Pacific, eastern Indian, and eastern Pacific. In small regions in the centers of these warm (and fresh) pools temperature even works against salinity to reduce seasonal stratification (Figures 2a and 3). Salinity and temperature play roughly equal roles in setting the stratification in many locations under the ITCZ, with $-7.5 < Tu_s < 7.5°$. A region of the Tropical Atlantic Ocean north of the Amazon River also has salinity playing a more important role than temperature, with $-22.5 < Tu_s < -7.5°$. Barrier layers are often found in many of these regions [e.g., *de Boyer Montégut et al.*, 2007], and there is sometimes a noticeable semiannual component in the annual cycle of mixed layer density, with temperature and salinity extrema sometimes out of phase.

[22] At higher latitudes, salinity also plays an increasingly important role, with $Tu_s < -37.5°$ around Antarctica, and in most of the Arctic as well, except along the west coast of Northern Europe and Russia, where relatively warm, salty North Atlantic waters enter this marginal sea.

[23] Reprising, within the subtropics the seasonal Turner angle, Tu_s, is mostly near 45° (Figure 4b). Large temperature changes dominate the seasonal cycle there, resulting in large density changes (Figure 4a) that are stronger in the Northern Hemisphere. Around the tropics, where the trade winds blow, Tu_s increases, reflecting the influences of entrainment of fresher water within the seasonal pycnocline dominating over evaporative cooling to decrease salinity as temperature decreases within the mixed layer. In the tropics the seasonal mixed layer density change is small relative to the subtropics. Here both temperature and salinity can play a large role (often equal in the ITCZ) and salinity is dominant in establishing the seasonal density change in some locations, especially those where barrier layers are often found.

3.3. Phases of the Seasonal Mixed Layer Density Maxima and Minima

[24] The mixed layer density is usually at a maximum in hemispheric late winter to early spring (Figure 5a), generally sometime in March in the Northern Hemisphere and sometime in September in the Southern Hemisphere. The equatorial band and the North Indian Ocean are exceptions. However, the exact timing varies subtly with latitude (Figure 6, purple line), with maxima reached slightly prior to the spring equinox equatorward of about ±45°, and at or after the equinox poleward of those latitudes, at least until reaching latitudes high enough that seasonal cycles in sea ice become important. The times of maximum mixed layer P (Figure 6, green line) lead those of maximum mixed layer density by a month or two outside the tropics. This lead occurs because mixed layer P sometimes shoals greatly during calm conditions in late winter while mixed layer

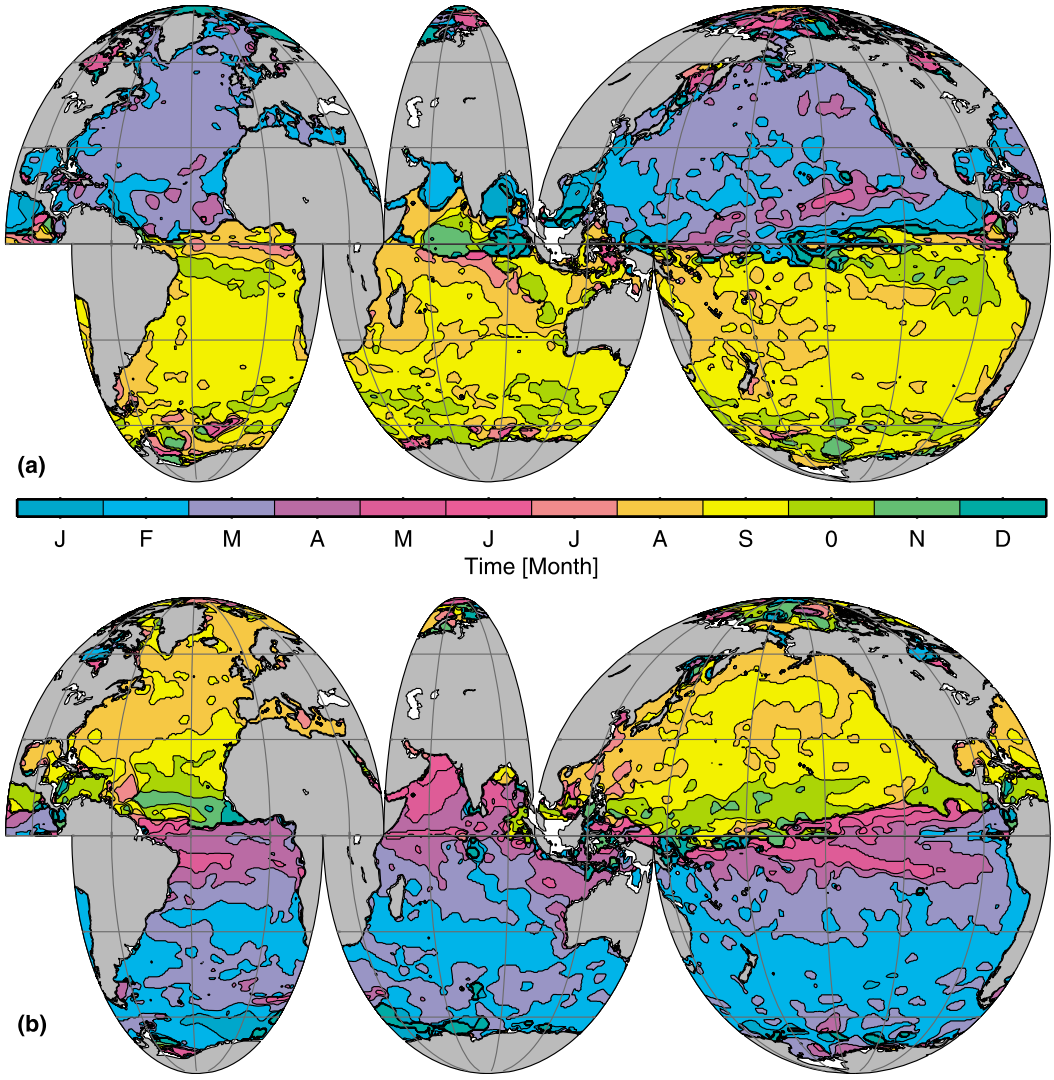

Figure 5. Maps of the month of (a) maximum and (b) minimum surface mixed layer density.

density only decreases slightly. In other words, mixed layer P does not exhibit a normal distribution, at least in late winter.

[25] Furthermore, there are regional differences (Figure 5a), with the trade wind regions in the eastern Pacific and Atlantic oceans, where barrier layers influence the seasonal cycle of the mixed layer [*Mignot et al.*, 2007], lagging by a month or more in reaching their maximum density. The equatorial upwelling regions lead the Southern Hemisphere timing by a few months, presumably because of the influence of Southern Hemisphere trade winds extending north of the equator, the timing of the upwelling season, and the relatively small seasonal changes in insolation. Equatorial barrier layers [e.g., *Sprintall and Tomczak*, 1992; *Mignot et al.*, 2007] may also influence the seasonal cycle in some locations. Also, the western Arabian Sea south of Oman has a maximum density in August (despite its Northern Hemisphere location) toward the end of the Southwest Monsoon, presumably because of evaporative cooling and entrainment of colder waters from below by the strong monsoon winds, as well as coastal upwelling. Finally, while the maximum mixed layer density appears to be achieved over a wide range of months in the Arctic, seasonal coverage in much of the Arctic is not optimal, and sea ice and river discharge complicate matters, so these times may not be well determined.

[26] The times at which the mixed layer density is at a minimum outside of the equatorial band and the North Indian Ocean are usually late summer to early fall (Figure 5b), as expected, generally sometime in August–September in the Northern Hemisphere and sometime from February to April in the Southern Hemisphere. For these times the change in seasonal phasing with latitude is quite pronounced (Figure 6, orange line), with minimum density occurring sometime after the fall equinox for within 5–15° from either side of the equator, and increasingly prior to the equinox going poleward of ±15° from the equator, at least to about ±70°.

[27] Once again, there are regional patterns in this seasonal phasing. Minimum mixed layer density in the eastern equatorial Pacific and Atlantic is shifted a few months early of surroundings owing to reduced upwelling around January, and the shift from austral to boreal fall again occurs north of the equator for the ocean mixed layer density. In the

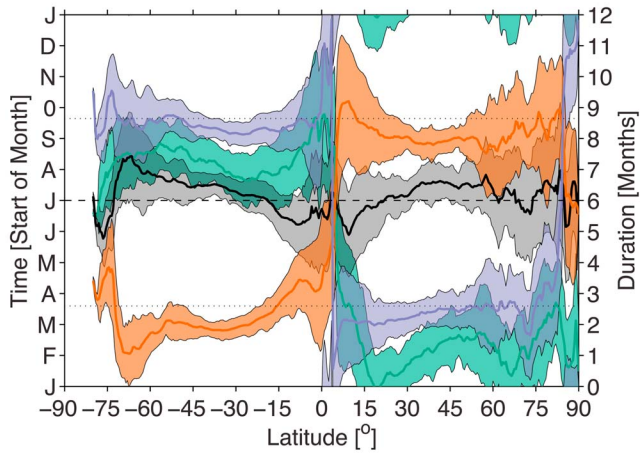

Figure 6. Circular means (lines) with one circular standard deviation envelopes (shaded regions) at each latitude for times of maximum mixed layer density (purple), times of maximum mixed layer P (green), times of the minimum mixed layer density (orange), and duration of the buoyancy loss season (black). Equinoxes (dotted lines associated with left axis and colored lines) and six-month duration time (dashed lined associated with right axis and black line) are indicated.

North Indian Ocean, the minimum mixed layer density is found in May–June, except in the northern Bay of Bengal where the freshening influence of river runoff shifts it into October (Figure 5b). The region north of the Amazon has a minimum in density in July, quite different from surrounding regions and a few months after the May seasonal maximum of Amazon discharge [*Zeng*, 1999], consonant with the dominant role of salinity in setting the seasonal stratification there (Figure 3). Again, the Arctic Ocean shows a wide range of values, but between poor data coverage and seasonal ice issues they may be uncertain.

[28] The length of the buoyancy loss season (Figure 6, black line) is shorter than six months within about ±20° of the equator—as short as five months in the mean at some of the very low, but off-equatorial latitudes, mostly because of the late fall timing of the density minimum. Some of these regions have prominent semiannual signals in the seasonal density cycle, and some have noteworthy barrier layers [*Mignot et al.*, 2007]. Combined with small density changes (Figure 2c), this semiannual energy leads to higher variability and uncertainties in the annual analysis presented here. The length of the buoyancy loss (cooling) season generally exceeds six months poleward of ±20° from the equator, approaching seven months in some places, at least until very high latitudes where the influences of seasonal cycles in sea and continental ice become prevalent and sampling is poor in some places. This asymmetry might be in part because of the asymmetry in mixed layer evolution (with a rapid spring shoaling and warming due to restratification, but a longer, slower cooling and deepening due to entrainment). It might also be related to the maximum in poleward heat transport by the oceans near ±20° from the equator [e.g., *Ganachaud and Wunsch*, 2000], so that the ocean warms for more of the year near the equator and carries heat toward the poles, where it gives it up by cooling for more of the year.

3.4. Horizontal Density Gradients and Turner Angle at the Times of Maximum Mixed Layer Density

[29] As noted above, the ocean surface mixed layer communicates most effectively with the interior ocean at the time of maximum mixed layer density, making this time worthy of special attention. The magnitude of the horizontal mixed layer density gradient at these times (Figure 7a) reveals where large fronts separate different water masses and where winter mixed layer density is more homogenous, whereas the component of the horizontal Turner angle parallel to the direction of the surface density gradient, Tu_h, reveals how mixed layer temperature and salinity distributions interact to reinforce these fronts, or to reduce density gradients (Figure 7b).

[30] Some of the strongest and most noticeable density fronts run east–west just north of the equator in the eastern Atlantic and Pacific oceans (Figures 7a and 8a), where the cold, relatively salty water upwelling on the equator and the warmer fresher water in the ITCZ converge [e.g., *Yoder et al.*, 1994], so both temperature and salinity gradients contribute to the density gradient (Figures 7b and 8b). The equatorial regions, with their otherwise relatively weak horizontal mixed layer density gradients (Figures 7a and 8a), exhibit a wide range of Tu_h (Figures 7b and 8b).

[31] The subtropical salinity maxima (Figure 1b) are centered near ±15° from the equator except in the South Indian Ocean, where the maximum is poleward of 30°S. There are large patches in the subtropics where $Tu_h > 52.5°$ (or in a few smaller regions $Tu_h < -52.5°$) at the time of maximum mixed layer density (Figures 7b and 8b), and in some parts of these regions, $Tu_h > 82.5°$ (or in a few smaller parts $Tu_h < -82.5°$). In these regions, generally poleward freshening works to partially offset poleward decreases in temperature, so horizontal density gradients are small (Figures 7a and 8a). Equatorward of these subtropical salinity maxima, temperature increases equatorward and salinity decreases, making for $-37.5 < Tu_h < 37.5°$ (Figures 7b and 8b). This pattern holds from the subtropical salinity maxima to the ITCZ and SPCZ in the Atlantic and Pacific oceans, so mixed layer horizontal temperature and salinity gradients work constructively in terms of their contributions to density in these transition regions and stronger horizontal density gradients result (Figures 7a and 8a). The high density-gradient region in the South Indian Ocean between the warm, fresh Indonesian Throughflow and the colder, saltier subtropical salinity maximum from 15°S to 30°S is especially wide and prominent.

[32] The meridional salinity minimum along ~40°S in the Pacific (Figure 1b), prominent in the east, sets up another region of weak density gradient with compensating temperature and salinity gradients to its north, and a region of strong density gradient to its south because of constructive temperature and salinity gradients (Figure 7).

[33] In the Bay of Bengal and eastern Arabian Sea, negative Tu_h (Figure 7b) shows that salinity (Figure 1b) dominates the horizontal density structure, whereas in the western Arabian Sea, positive Tu_h (Figure 7b) reflects the

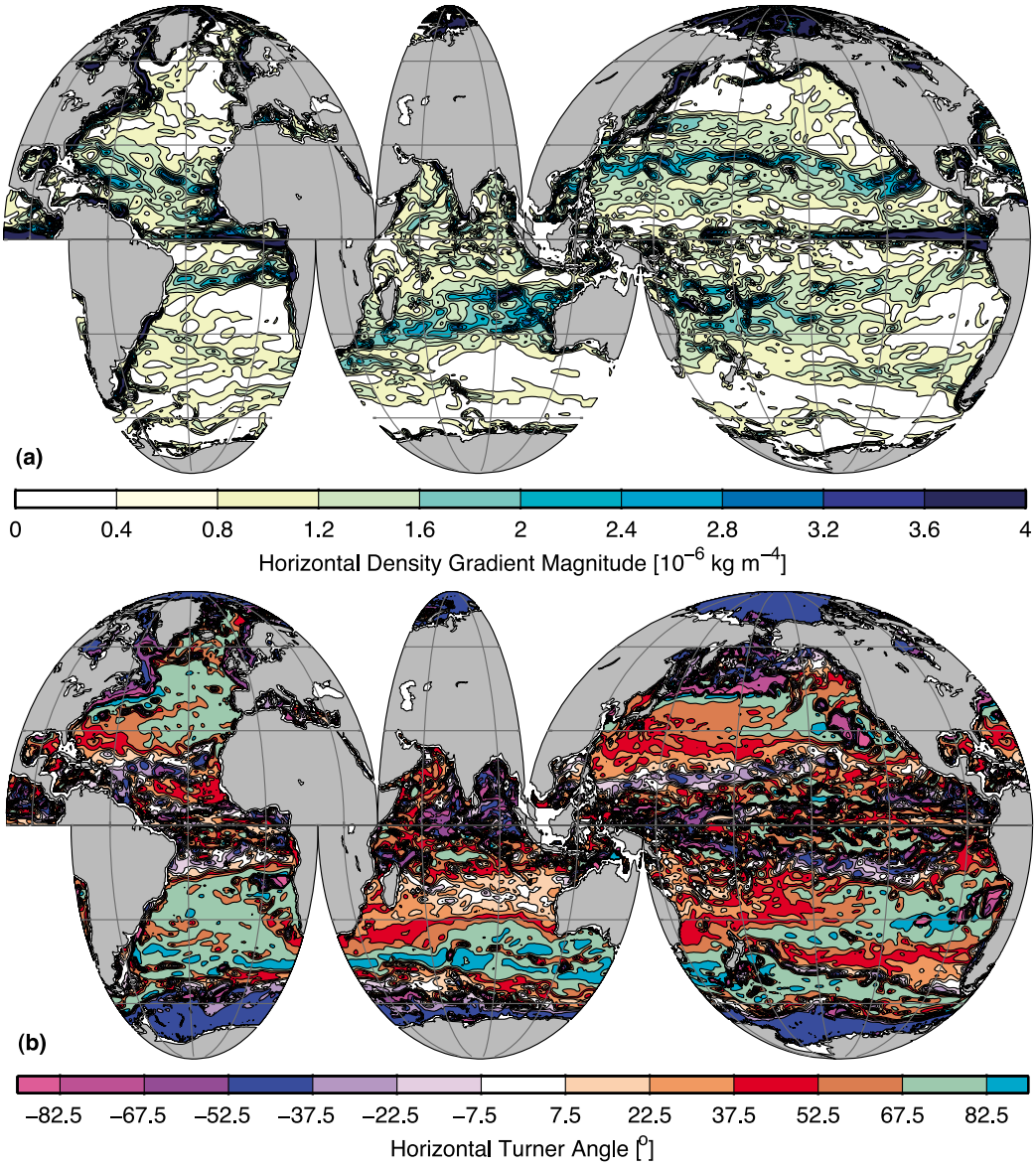

Figure 7. Maps of (a) horizontal density gradient magnitude and (b) horizontal Turner angle at times of the maximum surface mixed layer density.

fact that temperature (Figure 1a) gradients are the stronger contributor to the horizontal density gradients, although the density gradient is largest (Figure 7a) in the region between where both T and S gradients contribute constructively to the density gradient (Figure 7b).

[34] Another region where cold, fresh water meets warmer, salty water is in the confluence of the Kurushio and Oyashio, in the western North Pacific [e.g., *Roden*, 1977]. In this region, the magnitude of Tu_h is large, with signs both positive and negative (Figure 7b), whereas the horizontal density gradient is small (Figure 7a). This density-compensating region extends from Japan to at least 150°W.

[35] Again, temperature gradients (Figure 1a) persist along the Atlantic inflow to the Arctic, creating positive Tu_h (Figure 7b), but in the rest of the Arctic, salinity gradients dominate (Figures 7b and 8b). Similarly, in the Antarctic, where horizontal temperature gradients are very small, Tu_h is negative, with salinity dominating. However, a band of significant density gradient running roughly east–west (but trending generally south except for northward excursions near Drake Passage, the Kerguelen Plateau, and the Pacific-Antarctic Ridge) can be seen along much of the Antarctic Circumpolar Current (Figure 7a). Across this front, salinity and temperature both contribute to the density gradient (Figure 7b), with colder, slightly saltier (perhaps owing to the influence of upwelling [e.g., *Speer et al.*, 2000]) water to the south and warmer, slightly fresher water to the north.

4. Discussion

[36] Bivariate censuses of Tu_s and Tu_h versus density changes and horizontal density gradients, respectively, reveal some strong patterns (Figure 9). Temperature plays a primary role in the seasonal change of density throughout the bulk of the surface area of the world ocean, especially where that density change is large (Figure 9a), with 62% of

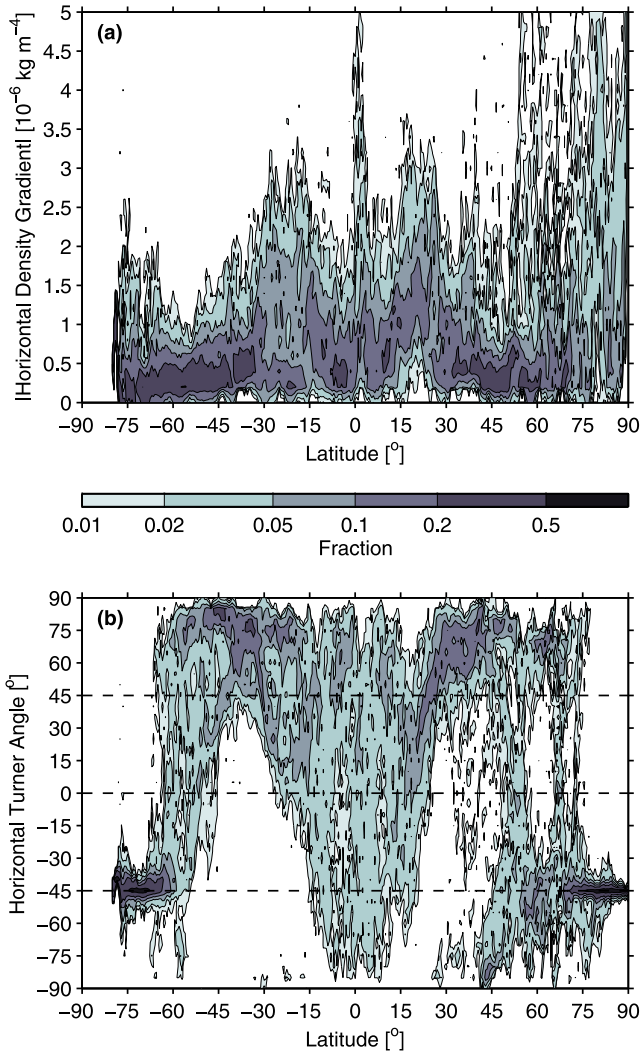

Figure 8. Fraction of surface mixed layer (a) horizontal density gradient magnitude in 0.2×10^{-6} kg m^{-4} bins and (b) horizontal Turner angle in 5° bins as a function of latitude, contoured at roughly logarithmic intervals.

the ocean surface within the 0.5% contour centered around $Tu_s = 45°$. Salinity is the most important contributor over a much smaller fraction of the ocean surface. The fraction of surface area where temperature and salinity both play a strong (and constructive) role is even smaller, and the seasonal density change is usually smaller in these regions. These latter two regions are largely coincident with locations where barrier layers are often present [e.g., *de Boyer Montégut et al.*, 2007]. A still smaller portion of the ocean surface area exists where the two water properties work against each other in the seasonal cycle, and again the seasonal density change in those areas is generally small.

[37] In contrast to the seasonal mixed layer changes, a fair fraction of the ocean's surface area at the times of maximum mixed layer density has temperature and salinity gradients that work against each other to reduce the horizontal density gradients (Figure 9b), with about 34% of the late winter ocean surface within the 0.5% contour present where $Tu_h \geq 42.5°$, and 10% of the late winter ocean surface having $Tu_h \geq 77.5°$. The most common occurrence of this condition is in regions of weak horizontal stratification, where the horizontal gradients in temperature are nearly (but not completely) compensated by horizontal salinity gradients, reducing the horizontal density gradients [*Rudnick and Ferrari*, 1999; *Ferrari and Rudnick*, 2000]. As these investigators note, horizontal mixing within the surface mixed layer will work to eliminate horizontal density gradients, but will not work as efficiently against compensated horizontal temperature and salinity gradients. However, this condition is far from universal. In the fraction of the ocean's surface where the mixed layer temperature and salinity work constructively, the horizontal density gradients at the time of the mixed layer maximum are generally stronger.

[38] The connection of the *T*–*S* relation of the late winter surface mixed layer to that in the ocean interior is an intriguing topic, especially in regions of high Tu_h [e.g., *Schmitt*, 1999]. As quantified globally here, late-winter

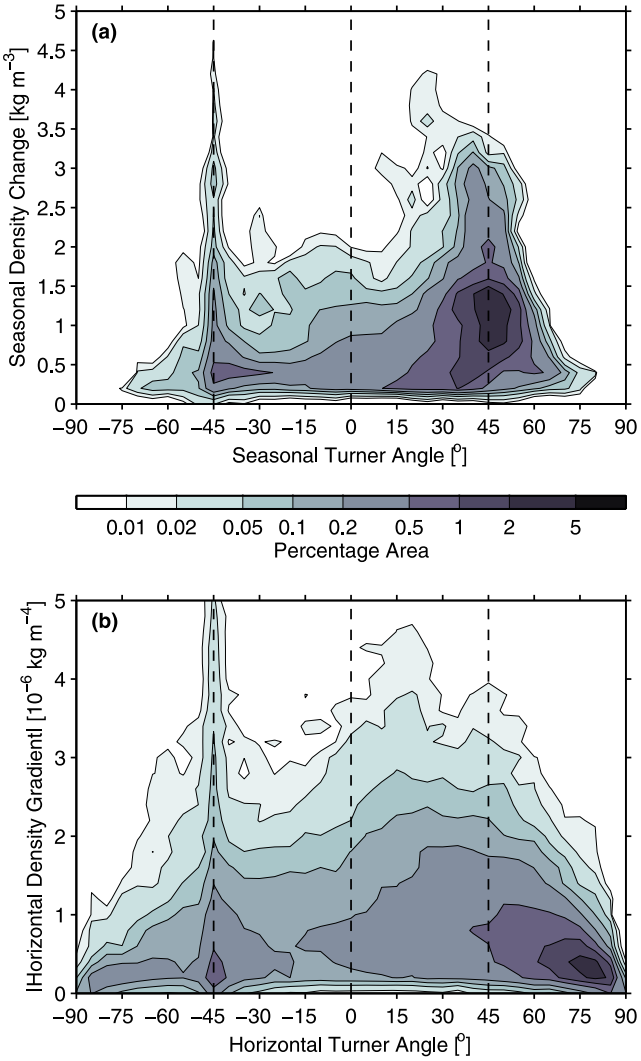

Figure 9. Percentage areas of surface mixed layer (a) seasonal Turner angle and seasonal density change in 5° by 0.2 kg m^{-3} bins and (b) horizontal Turner angle and horizontal density gradient magnitude at times of maximum density in 5° by 0.2×10^{-6} kg m^{-4} bins, contoured at roughly logarithmic intervals.

ocean mixed layers in the subtropics have $Tu_h > 82.5°$ in several locations (Figure 7b). However, in the ocean interior, vertical Turner angles >79° are rare and transient owing to strong salt fingering that works to eliminate them [*Rudnick and Ferrari*, 1999; *Schmitt*, 1999]. Late winter Tu_h values are quite high in the eastern subtropics of both hemispheres of the Atlantic and even more prominently in these regions of the Pacific, where eastern subtropical mode waters are subducted into the interior ocean [e.g., *Wong and Johnson*, 2003]. They are also high in the South Indian Ocean, where subantarctic mode waters are subducted [e.g., *Sallée et al.*, 2006]. The decay of high interior ocean Turner angles associated with mode water subduction, presumably by salt fingering, and the effects on interior ocean *T–S* relations has been investigated regionally on seasonal [e.g., *Sato and Suga*, 2009], interannual [e.g., *Johnson*, 2006], and decadal [e.g., *Johnson and Kearney*, 2009] timescales. This study quantifies the initial Turner angles for water subducted in these regions, as well as other regions around the world.

[39] **Acknowledgments.** NOAA Research and the NOAA Climate Program Office funded this work. The float data were collected and made freely available by the International Argo Program (part of the Global Ocean Observing System) and the national programs that contribute to it (see http://www.argo.ucsd.edu, http://argo.jcommops.org). G.C.J.'s week-long sojourn at the Helen Riaboff Whiteley Center, Friday Harbor Laboratories helped to germinate the manuscript. Comments from two anonymous reviewers and editor Frank Bryan helped to improve it. PMEL publication 3753.

References

Bakun, A., and C. S. Nelson (1991), The seasonal cycle of wind-stress curl in subtropical eastern boundary current regions, *J. Phys. Oceanogr.*, *21*, 1815–1834, doi:10.1175/1520-0485(1991)021<1815:TSCOWS>2.0.CO;2.

Boyer, T. P., et al. (2009), *World Ocean Database 2009, NOAA Atlas NESDIS*, vol. 66, edited by S. Levitus, 216 pp., U.S. Gov. Printing Office, Washington, D. C.

Bryden, H. L., J. Candela, and T. Kinder (1994), Exchange through the Strait of Gibraltar, *Prog. Oceanogr.*, *33*, 201–248, doi:10.1016/0079-6611(94)90028-0.

Chen, L. G. (1995), Mixed layer density ratio from the Levitus data, *J. Phys. Oceanogr.*, *25*, 691–701, doi:10.1175/1520-0485(1995)025<0691:MLDRFT>2.0.CO;2.

Coachman, L. K., and K. Aagaard (1988), Transports through Bering Strait: Annual and interannual variability, *J. Geophys. Res.*, *93*, 15,535–15,539, doi:10.1029/JC093iC12p15535.

Dai, A., and K. Trenberth (2002), Estimates of freshwater discharge from continents: Latitudinal and seasonal variations, *J. Hydrometeorol.*, *3*, 660–687, doi:10.1175/1525-7541(2002)003<0660:EOFDFC>2.0.CO;2.

de Boyer Montégut, C., G. Madec, A. S. Fischer, A. Lazar, and D. Iudicone (2004), Mixed layer depth over the global ocean: An examination of profile data and a profile-based climatology, *J. Geophys. Res.*, *109*, C12003, doi:10.1029/2004JC002378.

de Boyer Montégut, C., J. Mignot, A. Lazar, and S. Cravatte (2007), Control of salinity on the mixed layer depth in the world ocean: 1. General description, *J. Geophys. Res.*, *112*, C06011, doi:10.1029/2006JC003953.

Delcroix, T., C. Henin, V. Porte, and P. Arkin (1996), Precipitation and sea-surface salinity in the tropical Pacific Ocean, *Deep Sea Res., Part I*, *43*, 1123–1141, doi:10.1016/0967-0637(96)00048-9.

Fasham, M. J. R., H. W. Ducklow, and S. M. McKelvie (1990), A nitrogen-based model of plankton dynamics in the oceanic mixed layer, *J. Mar. Res.*, *48*, 591–639.

Ferrari, R., and D. L. Rudnick (2000), Thermohaline variability in the upper ocean, *J. Geophys. Res.*, *105*, 16,857–16,883, doi:10.1029/2000JC900057.

Ganachaud, A., and C. Wunsch (2000), Improved estimates of global ocean circulation, heat transport and mixing from hydrographic data, *Nature*, *408*, 453–457, doi:10.1038/35044048.

Gordon, A. L. (1989), Brazil-Malvinas Confluence–1984, *Deep Sea Res., Part A*, *36*, 359–384, doi:10.1016/0198-0149(89)90042-3.

Hagen, E., R. Feistel, J. J. Agenbag, and T. Ohde (2001), Seasonal and interannual changes in Intense Benguela Upwelling (1982–1999), *Oceanol. Acta*, *24*, 557–568, doi:10.1016/S0399-1784(01)01173-2.

Häkkinen, S. (1993), An Arctic source for the Great Salinity Anomaly: A simulation of the Arctic ice-ocean system for 1955–1975, *J. Geophys. Res.*, *98*, 16,397–16,410, doi:10.1029/93JC01504.

Han, W., and J. P. McCreary Jr. (2001), Modeling salinity distributions in the Indian Ocean, *J. Geophys. Res.*, *106*, 859–877, doi:10.1029/2000JC000316.

Hansen, B., and S. Osterhus (2000), North Atlantic–Nordic Seas exchanges, *Prog. Oceanogr.*, *45*, 109–208, doi:10.1016/S0079-6611(99)00052-X.

Holte, J., and L. Talley (2009), A new algorithm for finding mixed layer depths with applications to Argo data and subantarctic mode water formation, *J. Atmos. Oceanic Technol.*, *26*, 1920–1939, doi:10.1175/2009JTECHO543.1.

Hosegood, P. J., M. C. Gregg, and M. H. Alford (2008), Restratification of the surface mixed layer with submesoscale lateral density gradients: Diagnosing the importance of the horizontal dimension, *J. Phys. Oceanogr.*, *38*, 2438–2460, doi:10.1175/2008JPO3843.1.

Jenkins, W. J. (1982), On the climate of a subtropical ocean gyre: Decade timescale variations in water mass renewal in the Sargasso Sea, *J. Mar. Res.*, *40*, 265–290.

Johns, W. E., F. Yao, D. B. Olson, S. A. Josey, J. P. Grist, and D. A. Smeed (2003), Observations of seasonal exchange through the Straits of Hormuz and the inferred heat and freshwater budgets of the Persian Gulf, *J. Geophys. Res.*, *108*(C12), 3391, doi:10.1029/2003JC001881.

Johnson, G. C. (2006), Generation and initial evolution of a mode water θ–S anomaly, *J. Phys. Oceanogr.*, *36*, 739–751, doi:10.1175/JPO2895.1.

Johnson, G. C., and K. A. Kearney (2009), Ocean climate change fingerprints attenuated by salt fingering?, *Geophys. Res. Lett.*, *36*, L21603, doi:10.1029/2009GL040697.

Kara, A. B., P. A. Rochford, and H. E. Hurlburt (2003), Mixed layer depth variability over the global ocean, *J. Geophys. Res.*, *108*(C3), 3079, doi:10.1029/2000JC000736.

Kessler, W. S., L. M. Rothstein, and D. Chen (1998), The annual cycle of SST in the eastern tropical Pacific, diagnosed in an ocean GCM, *J. Clim.*, *11*, 777–799, doi:10.1175/1520-0442(1998)011<0777:TACOSI>2.0.CO;2.

Lukas, R., and E. Lindstrom (1991), The mixed layer of the western equatorial Pacific Ocean, *J. Geophys. Res.*, *96*, 3343–3357.

Lutjeharms, J. R. E., and R. C. Van Ballegooyen (1988), The retroflection of the Agulhas Current, *J. Phys. Oceanogr.*, *18*, 1570–1583, doi:10.1175/1520-0485(1988)018<1570:TROTAC>2.0.CO;2.

Marchesiello, P., J. C. McWilliams, and A. Shchepetkin (2003), Equilibrium structure and dynamics of the California Current System, *J. Phys. Oceanogr.*, *33*, 753–783, doi:10.1175/1520-0485(2003)33<753:ESADOT>2.0.CO;2.

Martinson, D. G. (1990), Evolution of the Southern Ocean winter mixed layer and sea ice: Open ocean deepwater formation and ventilation, *J. Geophys. Res.*, *95*, 11,641–11,654, doi:10.1029/JC095iC07p11641.

Mignot, J., C. de Boyer Montégut, A. Lazar, and S. Cravatte (2007), Control of salinity on the mixed layer depth in the world ocean: 2. Tropical areas, *J. Geophys. Res.*, *112*, C10010, doi:10.1029/2006JC003954.

Ohlmann, J. C., D. A. Siegel, and C. Gautier (1996), Ocean mixed layer radiant heating and solar penetration: A global analysis, *J. Clim.*, *9*, 2265–2280, doi:10.1175/1520-0442(1996)009<2265:OMLRHA>2.0.CO;2.

Peng, T.-H., T. Takahashi, and W. S. Broeker (1987), Seasonal variability of carbon dioxide, nutrients and oxygen in the northern North Atlantic surface water: Observations and a model, *Tellus, Ser. B*, *39*, 439–458, doi:10.1111/j.1600-0889.1987.tb00205.x.

Prasad, T. G. (2004), A comparison of mixed-layer dynamics between the Arabian Sea and Bay of Bengal: One-dimensional model results, *J. Geophys. Res.*, *109*, C03035, doi:10.1029/2003JC002000.

Price, J. F., R. A. Weller, and R. Pinkel (1986), Diurnal cycling: Observations and models of the upper ocean response to diurnal heating, cooling, and wind mixing, *J. Geophys. Res.*, *91*, 8411–8427, doi:10.1029/JC091iC07p08411.

Risien, C. M., and D. B. Chelton (2008), A global climatology of surface wind and wind stress fields from eight years of QuikSCAT scatterometer data, *J. Phys. Oceanogr.*, *38*, 2379–2413, doi:10.1175/2008JPO3881.1.

Roden, G. I. (1977), Oceanic subarctic fronts of the central Pacific: Structure of and response to atmospheric forcing, *J. Phys. Oceanogr.*, *7*, 761–778, doi:10.1175/1520-0485(1977)007<0761:OSFOTC>2.0.CO;2.

Roemmich, D., G. C. Johnson, S. Riser, R. Davis, J. Gilson, W. B. Owens, S. L. Garzoli, C. Schmid, and M. Ignaszewski (2009), The Argo Program: Observing the global oceans with profiling floats, *Oceanography*, *22*, 34–43, doi:10.5670/oceanog.2009.36.

Ruddick, B. R. (1983), A practical indicator of the stability of the water column to double-diffusive activity, *Deep Sea Res., Part A*, *30*, 1105–1107, doi:10.1016/0198-0149(83)90063-8.

Rudnick, D. L., and R. Ferrari (1999), Compensation of horizontal temperature and salinity gradients in the ocean mixed layer, *Science*, *283*, 526–529, doi:10.1126/science.283.5401.526.

Sallée, J.-B., N. Wienders, K. Speer, and R. Morrow (2006), Formation of subantarctic mode water in the southeastern Indian Ocean, *Ocean Dyn.*, *56*, 525–542, doi:10.1007/s10236-005-0054-x.

Sato, K., and T. Suga (2009), Structure and modification of the South Pacific eastern subtropical mode water, *J. Phys. Oceanogr.*, *39*, 1700–1714, doi:10.1175/2008JPO3940.1.

Schanze, J. J., R. W. Schmitt, and L. L. Yu (2010), The global oceanic freshwater cycle: A state-of-the-art quantification, *J. Mar. Res.*, *68*, 569–595, doi:10.1357/002224010794657164.

Schmitt, R. W. (1999), Spice and the demon, *Science*, *283*, 498–499, doi:10.1126/science.283.5401.498.

Serreze, M. C., A. P. Barrett, A. G. Slater, R. A. Woodgate, K. Aagaard, R. B. Lammers, M. Steele, R. Moritz, M. Meredith, and C. M. Lee (2006), The large-scale freshwater cycle of the Arctic, *J. Geophys. Res.*, *111*, C11010, doi:10.1029/2005JC003424.

Sobarzo, M., L. Bravo, D. Donoso, J. Garces-Vargas, and W. Schneider (2007), Coastal upwelling and seasonal cycles that influence the water column over the continental shelf off central Chile, *Prog. Oceanogr.*, *75*, 363–382, doi:10.1016/j.pocean.2007.08.022.

Speer, K., S. R. Rintoul, and B. Sloyan (2000), The diabatic Deacon cell, *J. Phys. Oceanogr.*, *30*, 3212–3222, doi:10.1175/1520-0485(2000)030<3212:TDDC>2.0.CO;2.

Sprintall, J., and M. Tomczak (1992), Evidence of the barrier layer in the surface layer of the tropics, *J. Geophys. Res.*, *97*, 7305–7316, doi:10.1029/92JC00407.

Stommel, H. (1979), Determination of water mass properties of water pumped down from the Ekman layer to the geostrophic flow below, *Proc. Natl. Acad. Sci. U. S. A.*, *76*, 3051–3055, doi:10.1073/pnas.76.7.3051.

Tippins, D., and M. Tomczak (2003), Meridional Turner angles and density compensation in the upper ocean, *Ocean Dyn.*, *53*, 332–342, doi:10.1007/s10236-003-0056-5.

Toole, J. M., R. A. Krishfield, M.-L. Timmermans, and A. Proshutinsky (2011), The ice-tethered profiler: Argo of the Arctic, *Oceanography*, *24*, 126–135, doi:10.5670/oceanog.2011.64.

Warren, B. A. (1983), Why is no deep water formed in the North Pacific?, *J. Mar. Res.*, *41*, 327–347, doi:10.1357/002224083788520207.

Wong, A. P. S., and G. C. Johnson (2003), South Pacific eastern subtropical mode water, *J. Phys. Oceanogr.*, *33*, 1493–1509, doi:10.1175/1520-0485(2003)033<1493:SPESMW>2.0.CO;2.

Yoder, J. A., S. G. Ackleson, R. T. Barber, P. Flament, and W. M. Balch (1994), A line in the sea, *Nature*, *371*, 689–692, doi:10.1038/371689a0.

Yu, L. (2011), A global relationship between the ocean water cycle and near-surface salinity, *J. Geophys. Res.*, *116*, C10025, doi:10.1029/2010JC006937.

Yu, L., and R. A. Weller (2007), Objectively analyzed air-sea heat fluxes for the global ice-free oceans (1981–2005), *Bull. Am. Meteorol. Soc.*, *88*, 527–539, doi:10.1175/BAMS-88-4-527.

Zeng, N. (1999), Seasonal cycle and interannual variability in the Amazon hydrologic cycle, *J. Geophys. Res.*, *104*, 9097–9106, doi:10.1029/1998JD200088.

G. C. Johnson, Pacific Marine Environmental Laboratory, NOAA, 7600 Sand Point Way NE, Bldg. 3, Seattle, WA 98115, USA. (gregory.c.johnson@noaa.gov)

J. M. Lyman, Joint Institute for Marine and Atmospheric Research, University of Hawai'i at Manoa, 1000 Pope Rd., Marine Science Bldg. 312, Honolulu, HI 96822, USA.

S. Schmidtko, School of Environmental Sciences, University of East Anglia, Norwich Research Park, Norwich NR4 7TJ, UK.